ARTICLES

Mapping surface plasmons on a single metallic nanoparticle

JAYSEN NELAYAH[1], MATHIEU KOCIAK[1], ODILE STÉPHAN[1]*, F. JAVIER GARCÍA DE ABAJO[2], MARCEL TENCÉ[1], LUC HENRARD[3], DARIO TAVERNA[1], ISABEL PASTORIZA-SANTOS[4], LUIS M. LIZ-MARZÁN[4] AND CHRISTIAN COLLIEX[1]

[1]Laboratoire de Physique des Solides, Bâtiment 510, CNRS UMR 8502, Université Paris Sud XI, F 91405 Orsay, France
[2]Instituto de Optica, CSIC, Serrano 121, 28006 Madrid, Spain
[3]Laboratoire de Physique du Solide, Facultés Universitaires Notre Dame de la Paix, Namur B-5000, Belgium
[4]Departamento de Química Física, Universidade de Vigo, 36310 Vigo, Spain
*e-mail: stephan@lps.u-psud.fr

Understanding how light interacts with matter at the nanometre scale is a fundamental issue in optoelectronics and nanophotonics. In particular, many applications (such as bio-sensing, cancer therapy and all-optical signal processing) rely on surface-bound optical excitations in metallic nanoparticles. However, so far no experimental technique has been capable of imaging localized optical excitations with sufficient resolution to reveal their dramatic spatial variation over one single nanoparticle. Here, we present a novel method applied on silver nanotriangles, achieving such resolution by recording maps of plasmons in the near-infrared/visible/ultraviolet domain using electron beams instead of photons. This method relies on the detection of plasmons as resonance peaks in the energy-loss spectra of subnanometre electron beams rastered on nanoparticles of well-defined geometrical parameters. This represents a significant improvement in the spatial resolution with which plasmonic modes can be imaged, and provides a powerful tool in the development of nanometre-level optics.

The remarkable optical characteristics of metallic nanoparticles observed over an extended domain, encompassing the visible range, have been investigated by many photonic spectroscopical techniques, including absorption/scattering/reflection optical spectroscopy (averaged over a whole homogeneous or inhomogeneous population of nano-objects in solution or on substrates)[1] and optical near-field microscopy[2]. In the latter case, enhanced electromagnetic field techniques have opened the possibility of recording the optical response of individual objects[3]. However, the results reported up to now are limited to a spatial resolution of about 50 nm. They exhibit sensitivity for analysing a single particle but have not reached the level of mapping local variations in its optical response. Consequently, exploring an alternative approach can open new avenues.

It is well known that the energy loss encountered by a fast electron travelling along a linear path at a constant speed through or close to an object yields information on the latter optical properties[4–6]. Combination of a subnanometre electron probe with access to the near-infrared/visible/ultraviolet range is in principle possible in an electron energy-loss spectroscopy (EELS) experiment in the context of a scanning transmission electron microscope (STEM). One specificity of this instrument is to allow multi-signal detection so that both energy-loss spectra and the associated projected mass signal (high-angle annular dark-field (HAADF) signal) can be acquired simultaneously for each probe position while scanning the probe over the region of interest. In parallel to the development of several theories predicting spectral features[7,8] as a function of the fast-electron position, EELS measurements of bulk and surface plasmons have been carried out over the

past two decades on a variety of nano-objects (see, for example, refs 9,10). Up to now, these measurements were generally limited to the ultraviolet spectral range (above 3 eV of energy loss)[9,11]. The few experiments demonstrating the detection of spectral features down to 2 eV were carried out with a resolution limited by the size of the electronic probe (10 nm at most) in EELS[12] and limited photon-counting statistics in related cathodoluminescence-like experiments[13]. One major limitation of the EELS technique is that the low-energy part of the spectrum is usually masked by the tail of the so-called zero-loss peak (ZLP), that is, the peak of electrons interacting elastically or encountering losses too small to be experimentally resolved (for example, phonons). Here, by relying on new instrumental and methodology developments, we demonstrate, on individual triangular silver nanoprisms, the feasibility of mapping the spatial variation of surface plasmon resonances in the near-infrared/visible/ultraviolet domain with a spatial accuracy of the order of $\lambda/40$, where λ is the wavelength of the related excitation.

Triangular silver nanoprisms were synthesized by light-induced aggregation of small (5.5 nm) Ag nanoparticles, following a method previously reported[14]. Most nanoprisms are equilateral with flat tops and bottoms (Fig. 1a, inset). The length of their sides ranges between about 20 and 300 nm and they are typically 10 nm thick (see the Supplementary Information).

The EELS measurements were carried out in a VG-HB501 STEM operated at 100 kV and fitted with a Gatan 666 spectrometer and a home-made detection system. Spectra were recorded using the so-called spectrum-imaging (spim) mode[15], in which the 1-nm-diameter focused electron probe is rastered, with a constant
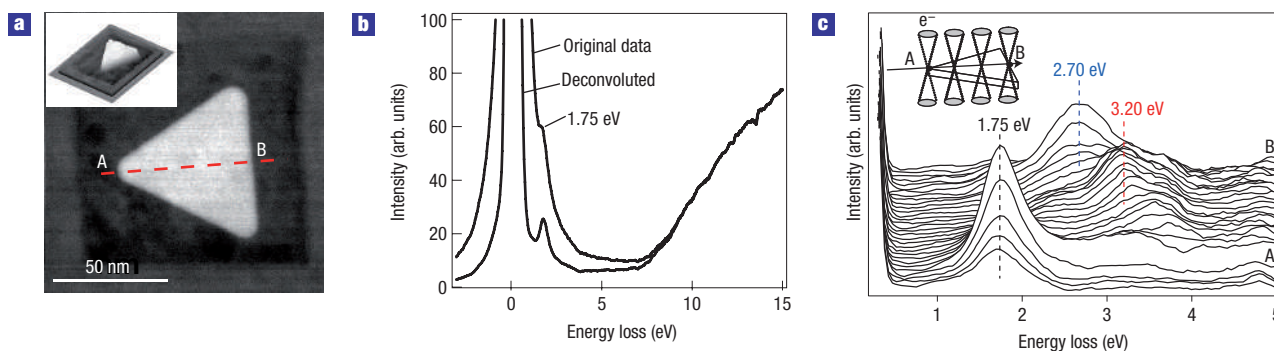
Figure 1 STEM–EELS measurements on an equilateral Ag nanoprism with 78-nm-long sides. **a**, HAADF–STEM image of the particle, showing the regular geometry that is characteristic of most triangular particles synthesized in this sample. The projected mass image of the scanned region shows the flat top and bottom morphology of the particle (inset). The image contrast around the particle is due to radiation damage in the mica caused by the electron beam. **b**, EEL spectra acquired at corner A before (raw data) and after deconvolution. After deconvolution, resonances (here, one peaked at 1.75 eV) in the ultraviolet/near-infrared domain are more clearly resolved. **c**, A series of 32 successive low-loss STEM–EEL spectra acquired, in the spectrum-image mode, along an axis (A to B) of the nanoprism as illustrated in the inset. The position of the three main resonances detected along the line scan are marked by dotted lines.
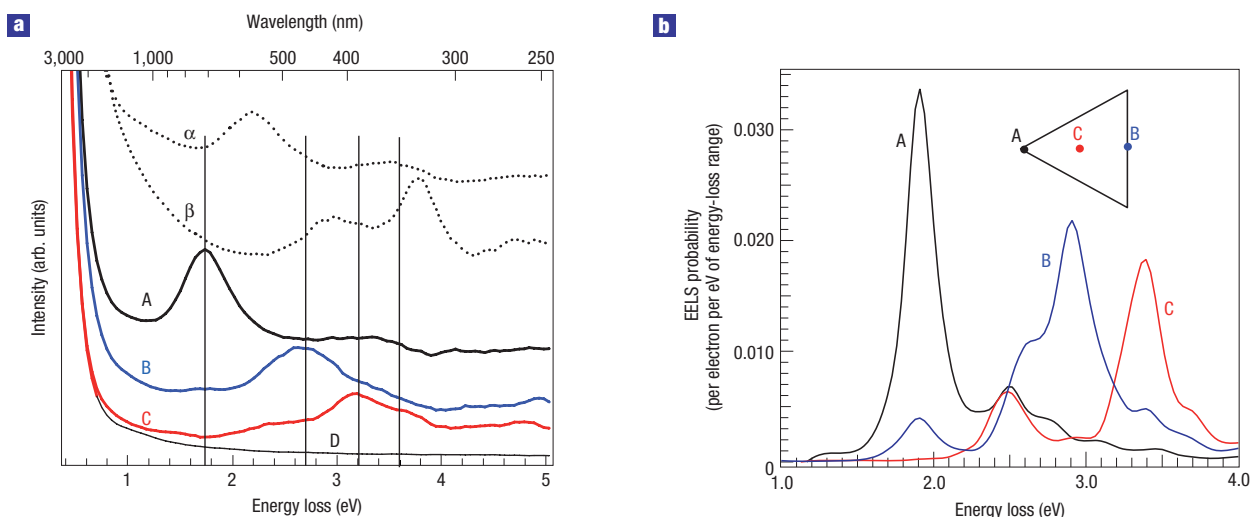

Figure 2 Experimental and simulated EEL spectra. **a**, Deconvoluted EEL spectra (solid lines) measured at (A) the corner (B) the edge and (C) the centre of the particle together with (D) the spectrum of the mica support. The last spectrum demonstrates the interest of the choice of a mica support that does not contribute at all to the EEL spectra over the energy domain of interest (1–5 eV). Spectra showing (α) the corner mode of a smaller equilateral triangular nanoprism and (β) the silver bulk mode (3.80 eV) and dipolar surface plasmon mode (3.00 eV) of a quasi-spherical Ag nanoparticle are also represented by dashed lines. The energy of the mode identified at the corners is size-dependent (compare spectra A and α). **b**, Simulated EEL spectra for a 10-nm-thick equilateral Ag nanoprism with 78-nm-long sides supported on mica at three impact parameters (A = triangle corner, B = triangle edge and C = triangle centre). Three major peaks at 1.9, 2.9 and 3.4 eV are seen at the corners, edges and centre of the particle respectively.

spatial displacement of 1–4 nm, over two-dimensional regions (typically 32×32 pixels) of the sample. At each point of the raster, a given number of spectra (typically 50) were acquired, with a dwell time per spectrum as short as 3 ms, in parallel with the HAADF signal shown in Fig. 1a. Figure 1c shows the evolution of the spectra as the electron probe is line-scanned along an axis of the nanoparticle. The fast acquisition rate of this detection system, together with the high brightness and small energy dispersion of the cold field-emission gun, made it possible to detect the presence of peaks at energies as low as about 1 eV, that is, in the near-infrared range (see Supplementary Information, Fig. S2). For easier quantitative analysis, a maximum-likelihood deconvolution scheme[16] was used and gave striking improvements in the

signal-to-background ratio for low-energy resonances (see Fig. 1b and Supplementary Information, Fig. S2).

Figure 2a shows deconvoluted EEL spectra at three distinct positions (A = triangle corner, B = triangle edge and C = triangle centre) on a 10-nm-thick equilateral triangular nanoprism with 78-nm-long sides. The spectra vary considerably from one position to the next. Four features are identified at 1.75, 2.70, 3.20 and 3.65 eV, respectively. In comparison, spectra acquired at the corner of a 25-nm-long equilateral nanoprism (curve α) and at the centre of a reference 20 nm quasi-spherical nanoparticle (curve β) from the same sample are represented by dotted lines. In the latter spectra, the Ag bulk plasmon at 3.80 eV (ref. 17) and a single surface plasmon at 3.00 eV are resolved, as expected for regular
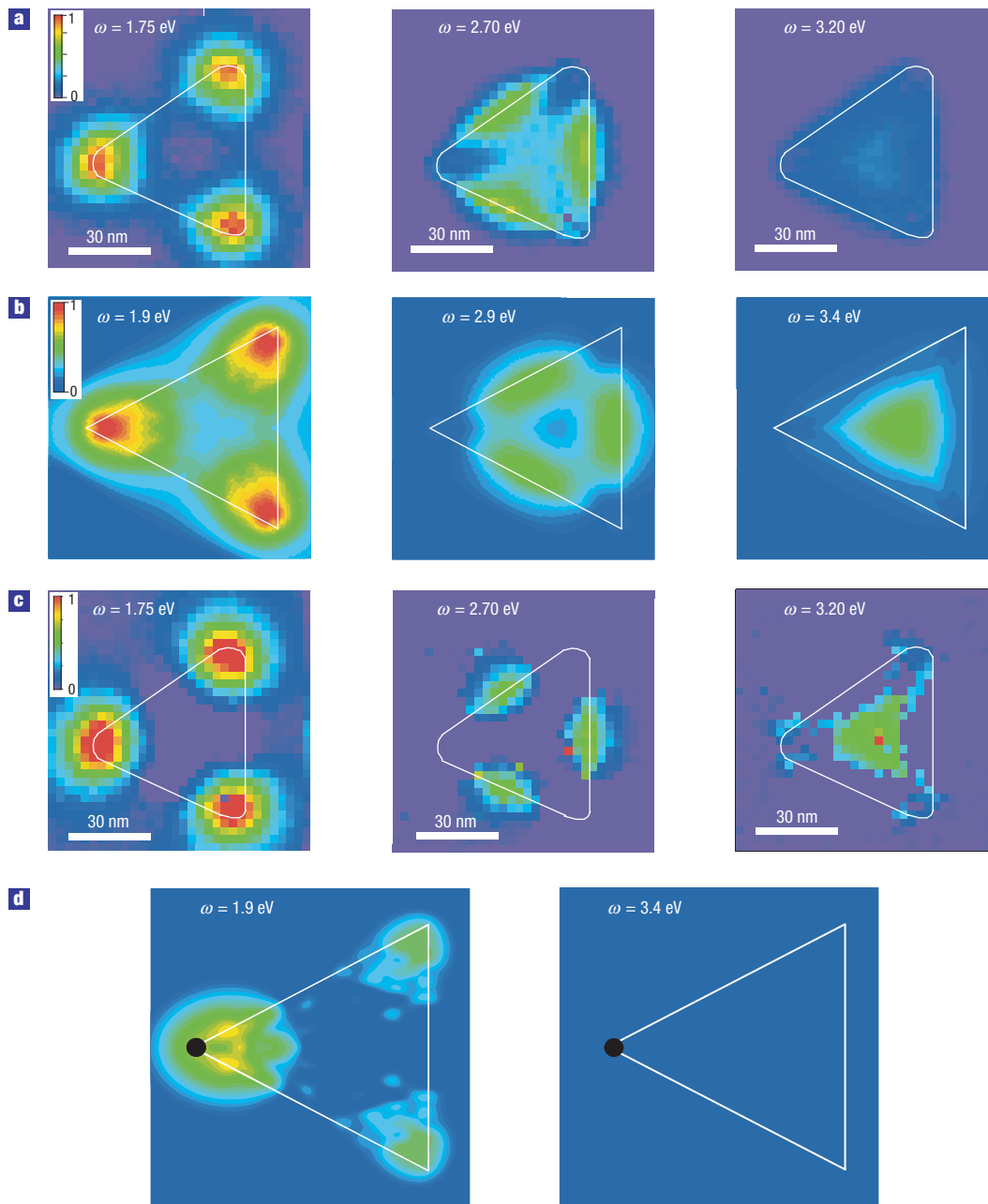
Figure 3 Experimental and simulated EELS amplitude maps. a, Distribution of the modes centred at 1.75, 2.70 and 3.20 eV respectively, in the spectra of the triangular particle shown in Fig. 2a. For each spectrum, the amplitudes of the modes are measured at their corresponding maxima after subtraction of the ZLP. The outer contour of the particle, deduced from its HAADF image, is shown as a white line. The colour scale, common to the three maps, is linear and in arbitrary units. **b**, Simulated amplitude maps of the three main resonances resolved in the simulated EEL spectra of the nanoprism with 78-nm-long sides. The colour linear scale, in arbitrary units, is common to the three maps. The simulated amplitude distributions for the different modes qualitatively match the experimental ones in **a**. **c**, EELS amplitude distributions obtained after gaussian fitting of the three modes mapped in **a**. The colour scale, common to the three maps, is linear and in arbitrary units (this scale is however different to the one in **a**). These maps were obtained by processing a 32×32 spectrum image. In each pixel, the amplitude of a given mode is deduced from the gaussian parameters. This method produces more well-localized spatial distributions as no artificial extension and background blurring of the modes is introduced during the analysis. **d**, Simulated induced near-field distribution around the particle at the resonance energy of 1.9 eV and at off-resonance energy of 3.4 eV for a probe (black circle) positioned at one corner. For the two maps, the square of the induced electric field is calculated at 3 nm above the nanoprism.

spherical silver nanoparticles[7,8]. For a given prism, the identified modes occur at fixed energies within the whole collection of spectra acquired (see Fig. 1c). By comparing the characteristics of these modes with previously published theoretical predictions

for individual triangular silver nanoprisms and related optical measurements on macroscopic sets[18] and individual nanoprisms[3], we can unambiguously identify the observed energy features as those of electromagnetic eigenmodes of nanoprisms. We have
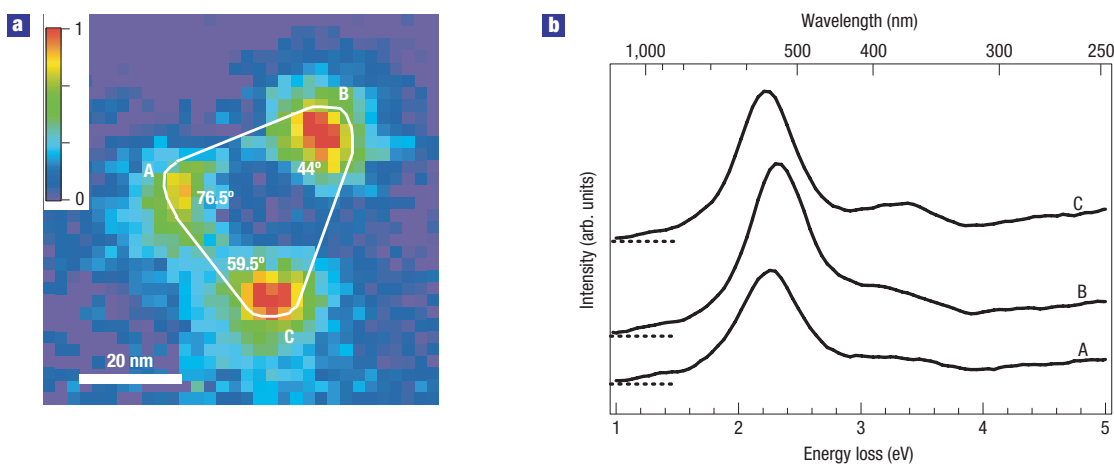
Figure 4 Experimental EELS study of an asymmetric triangular Ag nanoprism. a, EELS amplitude map of the mode dominating at the corners. The contour of the particle (white line) is shown together with the different values of the corner angles. The colour scale is in arbitrary units. The EELS intensity varies noticeably from one corner to another. The higher the angle of the corner, the less intense the mode is. **b**, Deconvoluted EEL spectra acquired at the three corners. The energy of the mode is almost fixed at 2.25 eV at each corner and the observed energy shifts are within experimental uncertainty.

also found that the three lower modes in energy are clearly size dependent, their energy decreasing for increasing edge length, as already observed experimentally for macroscopic sets of silver nanoprisms[14].

Significant variations in the relative intensities of the different modes are observed as the probe is scanned over the particle. This effect is quantified by an automatic estimate of the spectrum intensity at the maxima of the different resonances present in the spectral domain of interest. Applied to all of the spectra in a spectrum image, it enables, over the scanned area, a quick mapping of the amplitude distribution $P(\omega_i, x, y)$ of a given mode of pulsation ω_i. As exemplified by the particle shown in Fig. 1a, the amplitude distributions of the first three modes of silver nanoprisms exhibit a typical threefold behaviour characteristic of equilateral triangular prisms. These modes peak respectively at the corners, the edges and centre of the particle (Fig. 3a). The highest energy mode is barely resolved even after deconvolution. It is also worth noting that the bulk mode is never observed. Alternatively, at each pixel, the spectrum can be analysed to automatically detect and fit, using gaussian functions, any resonance present in the energy domain of interest[19]. Figure 3c shows EELS amplitude maps generated after gaussian fitting of the spectra. These amplitude maps give qualitatively the same results as those generated without any fit. However, the distributions are sharper and more localized as they do not suffer from the spatial blurring and background due to the energy overlap of the modes.

Theoretical studies of plasmon resonances in nanoprisms have until now been limited to the case of light excitation[18,20]. To take into account the specific properties of plasmon excitation and detection using fast electrons, further theoretical analysis including actual calculations of EELS intensities are therefore necessary. Accordingly, we have carried out such spatially resolved EELS calculations using the boundary element method[21,22] to obtain both EEL spectra and EELS amplitude maps. No fitting parameter has been used and the dielectric function of silver was extracted from optical data[23]. Bulk losses for penetrating trajectories were described by using Lindhard's dielectric function, which incorporates spatial dispersion of the bulk response[24] and seems to account satisfactorily for the so-called Begrenzung effect (that is, the cancellation of bulk losses in favour of surface modes)

for particles of small sizes. Figure 2b shows EEL spectra simulated for a 10-nm-thick prism with 78-nm-long sides supported on a mica substrate ($\epsilon = 2.3$) for three impact positions. At each probe position, a main resonance is observed together with minor peaks. The simulated energies of the three main peaks are in excellent agreement with experimental ones. In particular, spectral features are well reproduced and the bulk signal has nearly disappeared owing to the Begrenzung effect. The 0.2 eV slight difference between experimental and simulated resonance energy is attributed to the rough experimental estimate of the thickness of the silver nanoprisms.

Figure 3b shows simulated amplitude maps at the different resonance energies resolved in Fig. 2b. The agreement with the experimental results is again excellent except that surface imperfections and non-local effects, unaccounted for in the theory, seem to limit the spatial extension of the plasmon modes closer to their maxima. To get a closer insight into the origin of the EELS amplitude, we have also simulated induced field maps for a fixed probe position (Fig. 3d). Maxima (respectively nodes) of the EELS maps at a given resonance frequency correspond to probe positions at which an eigenmode is excited (respectively is not excited) and the associated induced field is maximum (respectively minimum). Heuristically, the observed similarities suggest that the EELS signal maps the eigenmodes field distribution. Recently, it has been shown that for a translationally invariant system, the EELS signal could be related to the electromagnetic density of states[25]. A description relating the EELS signal and the local electromagnetic density of states in thin nearly planar systems, such as our nanoprisms, is under preparation. This quantity, already known to be measured in scanning near-field optical microscopy experiments[26,27], is defined as the sum of the square of the electric eigenmodes of the system, by analogy to the well-known concept of electronic density of states used in solid-state physics.

It is worth discussing at this point the range of interaction between an electron and a nanoprism. Although the electromagnetic field generated by the incoming electron decays quickly with distance from it, eigenmodes are excited over the whole nanoparticle, that is, over more than 70 nm in the present case (Fig. 3d). Our simulations show that the excited mode for a

given position on the particle is a stationary wave encompassing the whole particle and excited only at the resonance energy. This proves that, even if the excitation of the mode is not detectable experimentally beyond an electron beam–particle distance of approximately 15 nm, an electron close to the nanoprism has an influence that spans over a much larger area, yielding a more refined idea of the concept of delocalization of the interaction in EELS[28]. The global character of the measured plasmon eigenmodes is further evidenced by the influence of the triangle size on the resonance associated with the corner of the triangle (compare spectra A and α in Fig. 2a).

A similar analysis has been undertaken on an asymmetric prism (Fig. 4) to get insight into the effects of particle shape on the EELS features identified in the ultraviolet/visible/near-infrared domain for triangular silver nanoprisms. Although the number of mode energies is larger for an asymmetric prism than for equilateral ones owing to reduction in symmetry, a corner-localized, low-energy mode is still present (Fig. 4a). Its common resonance-energy value at the three different corners provides further evidence that the corner feature resolved in the EEL spectra is truly the signature of eigenmodes whose spatial extension involves the entire triangular silver prism and not just the effect of a trivial local field enhancement at the triangle corners, as already demonstrated in Fig. 3d. Furthermore, the degeneracy of the three corner modes of the symmetric triangles is broken here, but the resulting asymmetry-driven energy shift seems to be smaller than the modes width (Fig. 4b). Variations in intensity of the low-energy mode from one corner to another depend on the local sharpness.

When mapping the intensity variations of the different plasmon modes using our technique, the definition and estimation of the spatial resolution deserve some further comments. In near-field optical microscopies, it is of common practice to express this resolution in terms of a fraction of the wavelength of the excited optical mode. Taking as a resolution criterion the full-width at half-maximum of the spatial maxima of the lowest mode (18 nm for $\lambda \sim 709$ nm), we can conclude that a resolution of the order of $\lambda/40$ has been realized. However, the smoothness of the spatial variations of the measured surface plasmons does not allow us to determine the ultimate resolution of our technique. We see in Fig. 3a,c that in the present experiment, the smallest, noise-limited measurable spatial variations of the first mode is of the order of 9 nm (this is the distance over which a maximum can be detected out of the noise, or alternatively, the distance below which two maxima would not be resolved owing to noise in Fig. 3a,c). In the future, we expect the spatial resolution of the technique to be improved by better spatial sampling and a higher signal-to-noise ratio.

We believe that these results open a new avenue for the comprehension of plasmon physics and the development of plasmonic engineering. Moreover, further insight into the nature of such plasmons is expected to come from ongoing simultaneous EELS and cathodoluminescence measurements aimed at determining the coupling strength between specific plasmon modes and propagating light.

METHODS

CHEMICALS AND SYNTHESIS

The synthesis of Ag nanoprisms was carried out through the photoinduced aggregation method. Small silver nanoparticles were prepared via reduction of 0.1 mM $AgNO_3$ (99+%, Aldrich) aqueous solution (200 ml) with 2 ml of 0.5 mM $NaBH_4$ (99%, Aldrich) in the presence of 0.3 mM trisodium citrate (98%, Sigma) under vigorous stirring. Immediately after injection of the reducing agent, 2 ml of a 5 wt% aqueous solution of poly(vinylpyrrolidone) (MW 10,000, Fluka) was added. The growth of the nanoprisms was carried out inside a commercial photoreactor (Luzchem LZC-Vis). Sodium chloride

(NaCl, =99%) was purchased from Aldrich. Milli-Q deionized water (resistivity higher than 18 MΩ cm^{-1}) was used for all of the preparations. All of the chemicals were used without further purification.

The sample was prepared by depositing and drying a few drops of an aqueous solution of the nanoparticles on a freshly cleaved mica substrate (Agar Scientific). Nanoparticles of various shapes and sizes were randomly and sparsely distributed (see Supplementary Information, Fig. S1).

SCANNING TRANSMISSION ELECTRON MICROSCOPE

The VG-HB501 STEM is equipped with a tungsten cold field-emission gun. The beam convergence half angle was set to about 7.5 mrad. This corresponds to the formation of the smallest possible electron probe (1 nm in diameter) at the sample surface. The half angle of collection was limited to 6 mrad by using a 600 μm collector aperture. The post-column Gatan 666 parallel spectrometer has a maximum dispersion of 0.05 eV per channel. EEL spectra were recorded with a two-dimensional charge-coupled device camera ($1,340 \times 100$ pixels) optically coupled to a scintillator in the image plane of the Gatan magnetic sector. The initial energy resolution of the EEL spectra is about 0.3–0.4 eV.

ELECTRON ENERGY-LOSS SPECTRA ACQUISITION AND PROCESSING

Currently, the energy resolution is limited mainly by the imperfect monochromaticity of the primary electron source, aberrations of the spectrometer and instabilities of the accelerating voltage and the spectrometer due to the mains a.c. power supply. Post-acquisition numerical processing of the acquired data, on the basis of an image-restoration algorithm, the Richardson–Lucy algorithm, is used to improve energy resolution. It requires the measurement of the point spread function (PSF) corresponding to the energy spread of the primary electron source and aberrations of the spectrometer. This PSF is estimated by acquiring a spectrum in vacuum with conditions similar to those of the spectra to be deconvoluted. For an effective deconvolution, the main prerequisite is to minimize the influence of the spectrometer and accelerating voltage instabilities on the recorded spectra. This is achieved by choosing an acquisition time per spectrum much shorter than the period of oscillation of the mains frequency of the mains power supply (in France, it is 50 Hz corresponding to a period, $t \sim 20$ ms). In this way, the power supply is almost constant over the acquisition time of a spectrum and as a consequence, the extra broadening of the spectrum, introduced by the instability of the power supply, is minimized. After deconvolution, the restored spectra have an energy resolution of 0.2–0.3 eV comparable to that achieved with a monochromator on Ag nanoparticles.

At each point of the scan in the spim, 50 spectra were acquired in the low-loss region (<50 eV) with a dwell time of 3 ms per spectrum ($\sim 1/7$ the period of the mains power supply) and a charge-coupled-device binning of 1×10. The number of spectra per pixel and binning conditions were chosen as a compromise between a substantial signal-to-noise ratio and a reasonable acquisition time per spim (with the present conditions, the acquisition time was about 15 min per spim) to avoid major sample drift during the scan of the focused electron beam. Each set of 50 spectra is then re-aligned, summed and deconvoluted. For each spim, a ZLP (that is, the PSF) is acquired by summing 300 spectra in vacuum with an acquisition time of 3 ms per spectrum. The number of iterations in the restoration process was set to four to avoid the introduction of artefacts (see Supplementary Information, Fig. S2).

The semi-automatized home-made routine for spectrum analysis was implemented using IGOR Pro 5.0 software (WaveMetrics) and works as follows. First, after deconvolution, the ZLP of the analysed spectrum is fitted and subtracted using an experimental ZLP acquired in vacuum. Consequently, modes present in the energy domain of interest are more clearly evidenced. The amplitude is then estimated as explained in the main text. When this process is repeated for all of the spectra of a spim, the amplitude of the different modes can be mapped at the nanometre scale over a given particle. To account for the intensity variation in the EELS signal over a spim, the amplitude of the different modes is normalized at each point of the raster. This is achieved by dividing its value by the total intensity under the corresponding EEL spectrum. The main pre-requisite for using the present amplitude mapping method is that the energies of the modes remain fixed from one probe position to another. The simulated EELS maps have been generated in a similar way from the simulated EEL spectra.

The above routine has also been run to automatically detect and fit the different modes present in the EEL spectra. After subtraction of the ZLP, any modes present in the analysed spectral domain are fitted by gaussian functions.

The fit parameters give direct access to characteristics such as the energy position, width and amplitude of the different modes at a given probe position. Nanoscale mapping of the above characteristics are obtained by repeating this process over a spim. It is worth noting that the energy maps generated have been used to ascertain that the energies of the modes are independent of probe position.

References

1. Hao, E., Schatz, G. C. & Hupp, J. T. Synthesis and optical properties of anisotropic metal nanoparticles. *J. Fluoresc.* **14**, 331–341 (2004).
2. Krenn, J. R. *et al.* Squeezing the optical near-field zone by plasmon coupling of metallic nanoparticles. *Phys. Rev. Lett.* **82**, 2590–2593 (1999).
3. Sherry, L., Jin, R., Mirkin, C., Schatz, G. & VanDuyne, R. Localized surface plasmon resonance spectroscopy of single silver triangular nanoprisms. *Nano Lett.* **6**, 2060–2065 (2006).
4. Ritchie, R. H. Plasma losses by fast electrons in thin films. *Phys. Rev.* **106**, 874–881 (1957).
5. Chen, C. H., Silcox, J. & Vincent, R. Electron-energy losses in silicon: Bulk and surface plasmons and Čerenkov radiation. *Phys. Rev. B* **12**, 64–71 (1973).
6. Raether, H. *Surface Plasmons on Smooth and Rough Surfaces and on Gratings* (Springer Tracts in Modern Physics, Vol. 111, Springer, Berlin, 1988).
7. Ferrell, T. L. & Echenique, P. M. Generation of surface excitations on dielectric spheres by an external elctron-beam. *Phys. Rev. Lett.* **55**, 1526–1529 (1985).
8. García de Abajo, F. J. Relativistic energy loss and induced photon emission in the interaction of a dielectric sphere with an external electron beam. *Phys. Rev. B* **59**, 3095–3107 (1999).
9. Batson, P. E. Surface plasmon coupling in clusters of small spheres. *Phys. Rev. Lett.* **49**, 936–940 (1982).
10. Ugarte, D., Colliex, C. & Trebbia, P. Surface-plasmon and interface-plasmon modes on small semiconducting spheres. *Phys. Rev. B* **45**, 4332–4343 (1992).
11. Arenal, R. *et al.* Electron energy loss spectroscopy measurement of the optical gaps on individual boron nitride single-walled and multiwalled nanotubes. *Phys. Rev. Lett.* **95**, 127601 (2005).
12. Khan, I. R. *et al.* A TEM and electron energy loss spectroscopy (EELS) investigation of active and inactive silver particles for surface enhanced resonance Raman spectroscopy (SERRS). *Faraday Discuss.* **132**, 171–178 (2006).
13. Yamamoto, N., Araya, K. & García de Abajo, F. J. Photon emission from silver particles induced by a high-energy electron beam. *Phys. Rev. B* **6420**, 205419 (2001).
14. Bastys, V., Pastoriza-Santos, I., Rodriguez-Gonzalez, B., Vaisnoras, R. & Liz-Marzan, L. M. Formation of silver nanoprisms with surface plasmons at communication wavelengths. *Adv. Funct. Mater.* **16**, 766–773 (2006).
15. Jeanguillaume, C. & Colliex, C. Spectrum-image: The next step in EELS digital acquisition and processing. *Ultramicroscopy* **28**, 252–257 (1989).
16. Gloter, A., Douiri, A., Tencé, M. & Colliex, C. Improving energy resolution of EELS spectra: An alternative to the monochromator solution. *Ultramicroscopy* **96**, 385–400 (2003).
17. Ouyang, F., Batson, P. & Isaacson, M. Quantum sizes effects in the surface-plasmon excitation of small metallic particles by electron-energy-loss spectroscopy. *Phys. Rev. B* **46**, 15421–15425 (1992).
18. Kelly, K. L., Coronado, E., Zhao, L. & Schatz, G. C. The optical properties of metal nanoparticles: The influence of size, shape, and dielectric environment. *J. Phys. Chem. B* **107**, 668–677 (2003).
19. Kociak, M., Stephan, O., Taverna, D., Nelayah, J. & Colliex, C. Probing surface plasmons on individual nano-objects by near-field electron energy loss spectroscopy. *Proc. SPIE* **5927**, 592711 (2005).
20. Hao, E. & Schatz, G. C. Electromagnetic fields around silver nanoparticles and dimers. *J. Chem. Phys.* **120**, 357–366 (2004).
21. García de Abajo, F. J. & Howie, A. Relativistic electron energy loss and electron-induced photon emission in lymphogenous dielectrics. *Phys. Rev. Lett.* **80**, 5180–5183 (1998).
22. García de Abajo, F. J. & Howie, A. Retarded field calculation of electron energy loss in inhomogeneous dielectrics. *Phys. Rev. B* **65**, 115418 (2002).
23. Johnson, P. B. & Christy, R. W. Optical constants of the noble metals. *Phys. Rev. B* **6**, 4370 (1972).
24. Lindhard, J. On the properties of a gas of charged particles. *K. Dan. Vidensk. Selsk. Mat.-Fys. Medd.* **28**, 1–57 (1954).
25. García de Abajo, F. J. *et al.* Cherenkov effect as a probe of photonic nanostructures. *Phys. Rev. Lett.* **91**, 143902 (2003).
26. Dereux, A., Girard, C. & Weeber, J. C. Theoretical principles of near-field optical microscopies and spectroscopies. *J. Chem. Phys.* **112**, 7775–7789 (2000).
27. Joulain, K., Carminati, R., Mulet, J. P. & Greffet, J. J. Definition and measurement of the local density of electromagnetic states close to an interface. *Phys. Rev. B* **68**, 245405 (2003).
28. Muller, D. A. & Silcox, J. Delocalization in inelastic-scattering. *Ultramicroscopy* **59**, 195–213 (1995).

Author contributions

This is a collective study in which members at (1) have mostly carried out experiments and measurements, members at (2) and (3) have mostly contributed to modelling and members at (4) have been responsible for the synthesis of the Ag nanoprisms.

Competing financial interests

The authors declare no competing financial interests.